9.2 A 0.6nJ -0.22/+0.19°C Inaccuracy Temperature Sensor Using Exponential Subthreshold Oscillation Dependence

Kaiyuan Yang, Qing Dong, Wanyeong Jung, Yiqun Zhang, Myungjoon Choi, David Blaauw, Dennis Sylvester

University of Michigan, Ann Arbor, MI

Thermal sensing is one of the most commonly desired features in IoT devices to monitor either environmental or system/chip conditions. An accurate temperature sensor usually requires carefully calibrated, high-accuracy ADCs, which prevents their use in ultra-low-power sensor nodes. In some sensing architectures, a highly accurate timing reference can replace the ADC [1]. With this in mind, we observe that almost all IoT systems incorporate a high-accuracy timing source (real-time clock, RTC) for time synchronization, data recording, and radio communication. Typically, these RTCs employ crystal or MEMS-based oscillators, or RC oscillators in extremely small form factor devices. We therefore propose to build a temperature sensor that uses a system's core RTC as a timing reference to minimize power/area overhead. We also show a fully integrated sensor that includes an RC-based timing circuit for systems that might not have a timing source.

Timing-based temperature sensors generally use oscillators to perform the sensing or analog-to-digital conversion, which is simple but has poor accuracy and voltage sensitivity compared to voltage-referenced designs [1]. In this work, we use a subthreshold oscillator as an exponential temperature-to-frequency converter, which reduces the impact of jitter of the sensing oscillator and reference timing source on sensor resolution, and also relaxes the requirement on the temperature stability of the timing reference. To accomplish this, we report: (1) an accurate fitting method derived from device models to transform the temperature dependence of subthreshold current to a linear output after 2-point calibration; (2) a subthreshold oscillator with stacked native NMOS header that achieves 1%/V (resulting in 0.13°C/V) line sensitivity; and (3) a delay cell with excellent current-to-frequency linearity to further improve accuracy across process variations. Pushing more processing to the digital domain can benefit from technology scaling and is especially suitable for IoT applications where data are transmitted to a server for processing. The power/area overhead of the temperature sensor (beyond the existing RTC) are 0.6nJ/conv at 125S/s and 8865μm^2 in 180nm CMOS. Despite the low costs, the temperature sensor achieves -0.22/0.19°C inaccuracy (3σ value) with crystal oscillator and –0.76/0.76°C with a fully integrated RC oscillator, 73/90mK resolution, and 0.13/0.36(°C/V) voltage sensitivity for the sensors with crystal/RC references.

A subthreshold oscillator is used as a sensing element to provide high temperature sensitivity with low power consumption (Fig. 9.2.1). The subthreshold temperature sensor in [2] fits temperature output with a simple exponential function. Instead, we derive a more accurate fitting model, given by equations in Fig. 9.2.1. Obtaining the two parameters in the model requires a 2-point calibration for each chip. A second major challenge with subthreshold oscillators is their high sensitivity to supply or bias voltage. To address this, we add a native NMOS (zero threshold voltage device) as a header device for the ring oscillator. This header behaves like a regulator with negative feedback. The regulated virtual VDD (VVDD) is determined by the V_{th} of the native header and the current drawn by the regulated oscillator. This voltage is around 300mV across temperature variations in our 180nm implementation. The oscillator current draw remains almost constant because of the staggered nature of oscillation and small on/off current ratio at deep subthreshold region, which helps stabilize VVDD. Cascading two native NMOS headers further improves oscillator line sensitivity. Pseudo-differential delay cells are used instead of single-ended inverters to further reduce fluctuation of current draw due to alternating switching of differential nets. Since we rely on the exponential temperature dependence of subthreshold currents for temperature conversion, oscillator frequency should be linear with device currents. We develop a delay cell with PMOS switches controlled by preceding stages to eliminate the impact of rising/falling slopes on oscillator frequency, ensuring it is highly linear with subthreshold current levels. The exponential dependence of frequency on temperature suppresses the impact of additional non-ideal noise and frequency shifts, which are linear terms, i.e., negligible (Fig. 9.2.2), resulting in very good noise-limited resolution and high accuracy, even with low-accuracy timing references.

The temperature sensor consists of a sensing ring oscillator, a timing reference, and sampling circuits (Fig. 9.2.3). Conventionally, frequency-to-digital converters are based on counting a sensing oscillator during a fixed number of reference cycles. This is not suitable for a sensing oscillator whose frequency depends exponentially on temperature, because its resolution and power consumption at high temperatures are orders of magnitude higher than that at lower temperatures, resulting in unbalanced performance across temperature and poor energy efficiency. Moreover, the sensing oscillator speed can be either lower or higher than a typical RTC frequency (10s of kHz) as temperature varies. To better scale sensor performance across temperature, we propose a sampling scheme that limits the number of cycles of the faster oscillator (Fig. 9.2.3). The circuit first finds the faster oscillator to reach programmable 2^N cycles and then waits for two additional cycles of the slower oscillator before stopping both counters. Thus, conversion time is bounded by $2^N \times T_{ref}$ and the quantization resolution is decided by the faster oscillator rather than the slower one. In addition, a counter underflow detector ensures a minimum of 2^n cycles on both counters before stopping them, ensuring enough conversion time.

To evaluate the temperature sensor in applications that cannot afford a crystal/MEMS oscillator, a frequency-locking-based RC oscillator [7] is implemented on-chip to evaluate the temperature sensor under worst-case timing reference (50 to 100ppm/°C and 0.5%/V). The timing reference can also be supplied by a 32.768kHz crystal oscillator on testing board, which experiences the same temperature as the sensor. To fully characterize the effects of process variation on accuracy of the temperature sensor, we test both TT chips and skewed corner chips. A total of 16 chips (8TT, 2FF, 2SS, 2FS, 2SF) are measured using the crystal oscillator frequency reference, showing excellent linearity of the sensing element. A single universal systematic error correction, rather than lot based correction, can be employed to improve the accuracy. Five integrated temperature sensors (one chip at each corner) are measured across temperature sweeps. As the on-chip resistor varies significantly at high temperatures, the operating range is reduced to –20 to 80°C, which is also the common operating range of RC oscillators. Because of limited number of samples (5 corners), the σ value is a very pessimistic estimation. Figure 9.2.4 plots the inaccuracy results of both versions.

As discussed above, the sensor suppresses noise significantly thanks to its exponential dependence on temperature, which is verified by measurements in Fig. 9.2.5. Since noise is significantly suppressed and the oscillators are running at low speed, the resolution is limited by quantization error. The rms resolution increases linearly with conversion time. 73 and 90mK rms resolution are achieved with crystal and RC oscillator with a practical 8ms conversion time. However, the best resolution FoM appears at 1 and 2 seconds for 70kHz RC oscillator and 32.768kHz crystal oscillator, which are 0.48pJ·K^2 for sensing core only using crystal and 1.73pJ·K^2 for fully integrated version.

Temperature sensors for IoT devices may operate under fluctuating supply voltages since power management on these devices is often limited due to lack of good passives or low power budgets. The stacked native header significantly improves ring oscillator line sensitivity. A voltage sensitivity of 0.13 and 0.36°C/V is achieved with crystal oscillator/RC timing references.

The 180nm temperature sensor core occupies 8865μm^2, which includes the sensing RO, counters, and state machine. The digital implementation makes the design very portable and highly scalable to new CMOS processes. The temperature sensor operates at 125 conversions/s while consuming 0.6 and 4.56nJ/conv. at 1.2V for sensing core only and fully integrated temperature sensor. Figure 9.2.6 summarizes measurements and compares to recent MOS-based low power temperature sensors. Figure 9.2.7 provides the die photo.

References:
[1] K.A.A. Makinwa, TU Delft, "Smart Temperature Sensor Survey," Rev. 19062016, June 2016. Accessed on Nov. 15, 2016.
<http://ei.ewi.tudelft.nl/docs/TSensor_survey.xls >.
[2] E. Saneyoshi, et al., "A 1.1V 35$\mu m \times 35\mu m$ Thermal Sensor with Supply Voltage Sensitivity of 2°C/10%-supply for Thermal Management on the SX-9 Supercomputer," *IEEE Symp. VLSI Circuits*, 2008.
[3] T. Anand, et al., "A Self-referenced VCO-based Temperature Sensor with 0.034°C/mV Supply Sensitivity in 65nm CMOS," *Symp. VLSI Circuits*, 2015.
[4] K. Souri, et al., "A 0.85V 600nW All-CMOS Temperature Sensor with an Inaccuracy of ±0.4°C (3σ) from -40 to 125°C," *ISSCC*, 2014.
[5] S. Jeong, et al., "A Fully-integrated 71nW CMOS Temperature Sensor for Low Power Wireless Sensor Nodes," *IEEE JSSC*, vol. 49, no. 8, pp.1682–1693, Aug. 2014.
[6] M. K. Law and A. Bermak, "A 405-nW CMOS Temperature Sensor Based on Linear MOS Operation," *IEEE TCAS-II*, vol. 56, no. 12, pp. 891–895, Dec. 2009.
[7] M. Choi, et al., "A 99nW 70.4kHz Resistive Frequency Locking On-chip Oscillator with 27.4ppm/°C Temperature Stability," *Symp. VLSI Circuits*, 2015.

Figure 9.2.1: Working principle of temperature-sensing ring oscillator with native NMOS header for better line sensitivity and linear fitting of sub-threshold current's temperature dependence.

Temperature Calculation based on counter outputs and reference frequency

$$T = \frac{b}{\ln(Freq) - a} = \frac{b}{\ln(count) - a - \ln(N) + \ln(Freq_{ref})}$$

$$= \frac{b}{\ln(count \times (1 + noise)) - a - \ln(N) + \ln(Freq_{ref} \times (1 + TC(T)))}$$

$$= \frac{b}{\ln(count) - a + \ln(Freq_{ref}/N) + \ln(1 + TC(T)) + \ln(1 + noise)}$$

Counter Outputs:

$$count = \frac{N \times Freq}{Freq_{ref}}$$

a and b are coefficients from 2-point calibration shown in Fig. 9.2.1

Temperature Coefficients of Timing Reference   Oscillator Noise

Both non-ideal terms linearly adds to the temperature error after attenuation by logarithm

Figure 9.2.2: Benefits of exponential frequency dependence based on theoretical analysis and empirical results by adding frequency offsets to measurement results.

Figure 9.2.3: System diagram with sampling scheme to improve resolution, and exemplary waveform.

Figure 9.2.4: Temperature sensor inaccuracy.

Figure 9.2.5: Supply sensitivity of sensing RO and rms/quantization resolution vs. conversion time.

	This work		VLSI' 15 [3]	ISSCC' 14 [4]	JSSC' 14 [5]	JSSC' 10 [6]
	Core	System				
Technology	180nm		65nm	160nm	180nm	180nm
Type	MOS		MOS	DTMOS	MOS	MOS
Digital Conversion	FDC		FDC	ZSD2	FDC	TDC
Fully Integrated	XO on board	Yes (RC Osc)	Yes	No*	Yes	External clock
Area (μm²)	8865	220000	4000	85000	90000	41600
Conversion Time (ms)	8	8	0.022	6	30	100
Power (μW)	0.075	0.57	154	0.6	0.071	0.12
Energy/Conversion (nJ)	0.6	4.56	3.388	3.6	2.13	3.6
Temperature Range (°C)	-20~100	-20~80	0~100	-40~125	0~100	-10~30
Inaccuracy (°C)	-0.22/0.19 (2-point)	-0.76/0.76 ** (2-point)	-0.9/0.9 (2-point)	-0.4/0.4 (1-point)	-1.4/1.5 (2-point)	-0.8/1 (2-point)
Resolution (mK)	73	90	300	63	300	200
Supply Voltage (V)	1.2	1.2	0.85~1.05	0.85	1.2	0.5
Voltage Sensitivity (°C/V)	0.13	0.36	34	0.45	14	Regulator
Resolution-FoM (pJ·K²)	3.2	36.9	304.92	14.29	191.7	144

* External OTA bias current and digital ADC backend.
** Estimated from only 5 chips at 5 corners, representing a pessimistic estimation.

Figure 9.2.6: Summary of measurement results and comparison with state-of-the-art MOS-based temperature sensors.
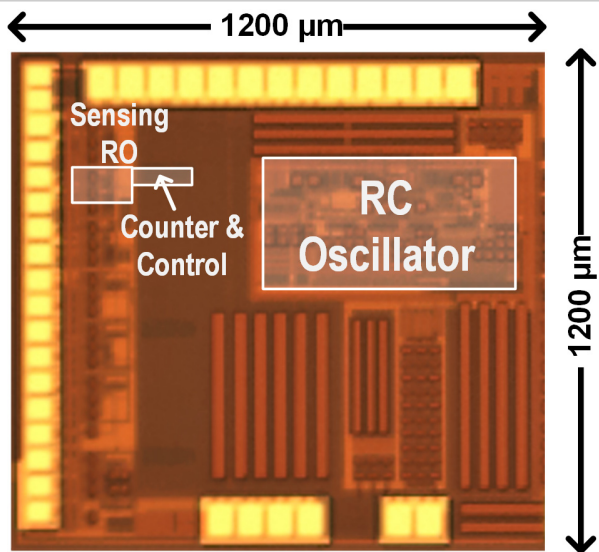
9

Figure 9.2.7: Die micrograph of 180nm temperature sensor.